Yeast Protein Farnesyltransferase: A Pre-Steady-State Kinetic Analysis†

Jeffery R. Mathis‡ and C. Dale Poulter*

Department of Chemistry, University of Utah, Salt Lake City, Utah 84112

Received November 26, 1996; Revised Manuscript Received March 10, 1997⊗

ABSTRACT: Protein farnesyltransferase catalyzes alkylation of the cysteine in a carboxy-terminal CaaX motif where a is typically an aliphatic amino acid and X is alanine, methionine, serine, glutamine, or cysteine by a farnesyl residue. The modification enhances the lipophilicity of farnesylated proteins and promotes their association with membranes as part of their normal cellular function. Among the proteins modified by farnesyl residues is Ras, an important component in the signal transduction network for cell division that has been implicated in several forms of human cancer. In this paper, we describe isotope trapping, rapid quench, and single turnover experiments with the yeast enzyme using farnesyl diphosphate and the short peptide RTRCVIA as substrates. The kinetic constants for substrate binding, chemistry, and product release were determined from a fit of the differential equations describing the minimal catalytic mechanism to the kinetic data by numerical integration. Rate constants for chemistry and product release were 10.5 and 3.5 s^{-1}, respectively. The dissociation rate constant (33 s^{-1}) for release of peptide from the ternary enzyme−substrate complex was three times larger than the rate constant for chemistry. The enthalpy of reaction, $\Delta H_{rxn} = -17 \pm 1$ kcal/mol for farnesylation of cysteine, was measured by microcalorimetry. Isotope trapping experiments revealed that the enzyme·farnesyl diphosphate complex was efficiently trapped by peptide but that the enzyme·peptide complex was not trapped by farnesyl diphosphate. These results are consistant with an ordered mechanism for formation of a catalytically competent ternary enzyme·farnesyl diphosphate·peptide complex.

The posttranslational modification of proteins with C_{15} farnesyl or C_{20} geranylgeranyl groups is a frequent occurrence in eukaryotic cells (Clarke, 1992; Rando, 1996). These modifications are essential for the function of the proteins and serve to promote protein−membrane or protein−protein interactions. Two different classes of protein prenyltransferases are known. The first consists of two enzymes that catalyze alkylation of the cysteine in carboxy-terminal CaaX motifs, where a is typically an aliphatic amino acid and X is the amino acid that determines whether the protein is a substrate for protein farnesyltransferase (PFTase)[1] or protein geranylgeranyltransferase-I (PGGTase-I). When X is alanine, methionine, serine, glutamine, or cysteine, the protein is farnesylated (Scheme 1), and when X is leucine, the protein is geranylgeranylated (Moores et al., 1991; Omer et al., 1993). The proteins that are substrates for these two enzymes include members of the Ras and Rho/Rac family of low molecular weight GTPases, γ-subunits of G proteins, nuclear lamins, G-protein-coupled receptor kinases, and retinal cGMP phosphodiesterase (Schafer et al., 1989). The CaaX motif is the major binding determinant for the protein substrates, and CaaX tetrapeptides are good alternate substrates for the two enzymes. The second class of protein prenyltransferases consists of a single enzyme, PGGTase-II, which catalyzes the alkylation of cysteines in carboxy-terminal CCXX, XXCC, and XCXC motifs in the Rab GTPases (Moores et al., 1991). In contrast to the protein prenyltransferases in the first class, PGGTase-II only recognizes Rab proteins as substrates when they are complexed with an escort protein.

Scheme 1: PFTase-Catalyzed Farnesylation of Cysteine

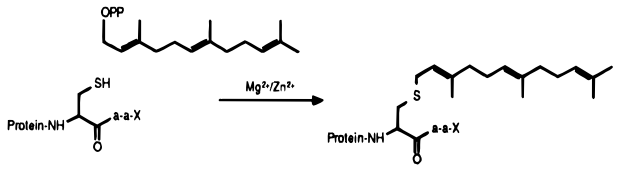

All three protein prenyltransferases are heterodimers composed of α- and β-subunits, and the enzymes show a substantial degree of similarity in their primary amino acid sequences (Omer et al., 1991). In addition, PFTase and PGGTase-I have the unusual property of sharing a common α-subunit. All of the protein prenyltransferases are metalloenzymes containing a tightly bound Zn^{2+} and also require Mg^{2+} for maximal activity. Recently, a second PFTase of considerably higher molecular mass (250 000 Da) was isolated from Burkitt lymphoma Daudi cells (Vogt et al., 1995). The β-subunit for the enzyme was immunologically indistinguishable from the β-subunit of other PFTases, but the α-subunit reacted poorly with a rat brain anti-α-antibody. In addition, the new PFTase retained a significant level of activity in the absence of Zn^{2+}, whereas Zn^{2+} was an absolute requirement for other PFTases (Reiss et al., 1992; Zhang et al., 1996).

Steady-state kinetic studies with mammalian PFTases suggested a random mechanism for substrate binding (Pom-

† This work was supported by NIH Merit Award 21328.
* To whom correspondence should be addressed.
‡ NIH Postdoctoral Fellow, GM17697.
⊗ Abstract published in *Advance ACS Abstracts,* May 1, 1997.

[1] Abbreviations: ACES, *N*-(2-acetamido)-2-aminoethanesulfonic acid; DTT, dithiothreitol; EDTA, ethylenediaminetetraacetic acid; FPP, farnesyl diphosphate; GGPP, geranylgeranyl diphosphate; HEPES, *N*-(2-hydroxyethyl)piperazine-*N*′-2-ethanesulfonic acid; PFTase, protein farnesyltransferase; PGGTase, protein geranylgeranyltransferase; PIPES, piperazine-*N*,*N*′-bis(2-ethanesulfonic acid); PP_i inorganic pyrophosphate; TFPP, 13-trifluorofarnesyl diphosphate; Tris, tris(hydroxymethyl)-aminomethane.

S0006-2960(96)02918-2 CCC: $14.00

pliano et al., 1992). Subsequent isotope trapping experiments conducted with recombinant human (Pompliano et al., 1993) and rat (Furfine et al., 1995) enzymes indicated that substrate binding was ordered, with the addition of FPP preceding the peptide. Stopped-flow fluorescence studies with rat PFTase suggested that farnesyl diphosphate (FPP) binds in a two-step process and that the peptide substrate binds to the E·FPP complex irreversibly (Furfine et al., 1995). In addition, a series of single-turnover experiments with limiting E·FPP showed that the rate constant for formation of enzyme-bound product was much faster that the catalytic rate constant (k_{cat}), indicating that catalysis was rate-limited by product release.

Yeast PFTase (Gomez et al., 1993; Mayer et al., 1993) is somewhat smaller than its mammalian counterparts. The primary amino acid sequence of the α-subunit in the yeast enzyme bears approximately 30% identity to mammalian proteins, while the identity in the β-subunit is slightly higher (Omer et al., 1993). In contrast to mammalian PFTases, steady-state kinetic measurements for the yeast enzyme gave typical double reciprocal plots consistent with an ordered mechanism where FPP binds before peptide (Dolence et al., 1995). In addition, the yeast enzyme was strongly inhibited by its peptide substrate. Although a similar phenomenon is seen in the double reciprocal plots for mammalian PFTases, the level of inhibition is much less pronounced. In this paper, we describe the results of isotope trapping and pre-steady-state kinetic experiments for yeast PFTase with a peptide substrate, RTRCVIA, which contains a RTR leader to facilitate separation of farnesylated peptide from unreacted FPP and the CVIA consensus sequence found in the yeast a-mating factor peptide, a normal substrate for the enzyme (Schafer et al., 1990). We have determined the individual rate constants for binding and release of substrates and the chemical step. In addition, we measured the enthalpy for farnesylation of cysteine by FPP using isothermal titration calorimetry. The large negative ΔH for the reaction suggests that the alkylation is irreversible.

MATERIALS AND METHODS

Materials. Recombinant yeast PFTase was obtained from *Escherichia coli* strain JM101/pGP114 and purified by ion-exchange and immunoaffinity chromatography as described previously (Mayer et al., 1993). Chromatographic fractions were analyzed by SDS−PAGE (MW = 77 kDa). Protein concentrations were determined by UV spectroscopy using a calculated extinction coefficient for PFTase $\epsilon = 1.99$ mL mg^{-1} cm^{-1} (153 340 M^{-1} cm^{-1}) at 280 nm based on the number of tyrosine and tryptophan residues (Gill & von Hippel, 1989) in the heterodimer. Concentrations determined by this procedure agreed closely with those from a Bradford assay (Bradford, 1976). Specific activities measured for different batches of purified yeast PFTase used in both calorimetric and kinetic experiments were from 2.9 to 3.6 μmol min^{-1} mg^{-1}, as determined by a spectrofluorimetric assay (Cassidy et al., 1995) using dansyl-GCVIA as the peptide substrate. The purified enzyme was stored in solution on ice until needed. Little or no loss of activity was observed over the course of 2 weeks.

Peptides RTRCVIA and dansyl-GCVIA were synthesized at the core facility of the University of Utah using solid-phase peptide methods. Concentrations of stock solutions, prepared by dissolving the peptide in water, were determined by sulfhydryl analysis using dithiobisnitrobenzoic acid (Russo & Bump, 1988). Stock solutions were combined with 5 mM DTT to a final concentration of 2−8 mM and stored at −20 °C. FPP was synthesized by the method of Davisson et al. (1986). 13-Trifluorofarnesyl diphosphate (TFPP) was synthesized by Dr. Julia Dolence (Dolence & Poulter, 1995). Stock solutions of FPP and TFPP (2−5 mM) in 25 mM ammonium bicarbonate were stored at −20 °C until needed. Concentrations were determined by analysis for phosphate (Cassidy et al., 1995). [1-^{3}H]FPP (17.8 Ci/mmol) was purchased from DuPont-NEN (Boston, MA). Phosphocellulose P81 filter paper was from Whatman (Clifton, NJ). Dodecyl-β-D-maltoside was purchased from CalBiochem. All other chemicals were from Sigma (St. Louis, MO) or USB (Cleveland, OH) and used without further purification.

Enzyme Assay. The assay used for PFTase in our kinetic studies was essentially as described by Roskoski et al. (1994). [^{3}H]FPP (0.5−10 μM, 200−500 μCi/μmol) was incubated at 30.0 °C with RTRCVIA (0.5−30 μM) and PFTase (1−5 nM) in assay buffer containing 10 mM $MgCl_2$, 10 μM $ZnCl_2$, 5 mM DTT, and 0.04% (w/v) dodecyl-β-D-maltoside in a total volume of 50.0 μL of 50 mM buffer (PIPES, HEPES, ACES, or Tris) at pH = 7.0. Reactions were initiated by the addition of enzyme, quenched with 10 μL of 1.2 M HCl after 5−20 min, and placed on ice (final pH 0.8−1). Background reactions were conducted with reaction buffer in place of enzyme. A portion of the reaction mixture (30 μL) was spotted on a 1 × 3 cm strip of phosphocellulose P81 filter paper that had been numbered in pencil. The solution was allowed to permeate the paper for a few seconds before the strip was immersed in 1:1 75 mM H_3PO_4/95% ethanol (10 mL/strip). Additional reaction mixtures within an experimental run were spotted likewise and combined in the same wash solution. The strips were gently swirled on a rotary platform for 10 min, followed by two additional 10-min wash cycles with fresh wash solution. The individual wet strips were transferred to scintillation vials containing 10.0 mL of Cytoscint (ICN) and 0.5 mL of 6 M HCl.

Trapping of Enzyme-Bound Substrate. The E·FPP complex was trapped essentially as described by Rose (1980). A pulse solution containing PFTase (1.4 μM) and [^{3}H]FPP (200 nM, 1000 μCi/μmol) in 50 mM Tris reaction buffer was prepared in a 1.5-mL Eppendorf tube. Portions (25.0 μL) were transferred to 0.7-mL Eppendorf tubes. Chase solutions consisting of RTRCVIA (0.1−5.0 μM) and TFPP (75 μM) in 50 mM Tris reaction buffer were prepared in a complementary set of 1.5-mL Eppendorf tubes. The reaction mixtures were allowed to equilibrate at 30 °C for 15 min. A 25.0-μL portion of chase solution was combined with the pulse and vortexed for 3−5 s. Final reactant concentrations in the mixture were 100 nM [^{3}H]FPP, 700 nM PFTase, 0.05−2.5 μM RTRCVIA, and 35.0 μM TFPP. After vortexing, reactions were quenched by the addition of 10.0 μL of 1.2 M HCl and placed on ice. A 30.0-μL portion was removed and analyzed as described above. Blank reactions were obtained by substitution of reaction buffer for either RTRCVIA in the chase solution or enzyme in the pulse solution.

A similar experiment was performed for enzyme-bound RTRCVIA using dansyl-GCVIA as the chase reagent. Control experiments showed that farnesylated dansyl-GCVIA was not retained on the phosphocellusose paper. PFTase and RTRCVIA in 40 μL of buffer were incubated at 30 °C

for 15 min. A portion (20 μL) of a chase solution consisting of [^{3}H]FPP (1000 μCi/μmol) and excess dansyl-GCVIA was combined with the pulse solution, vortexed, quenched with 10.0 μL of 1.2 M HCl, and placed on ice. Final concentrations were 250 nM enzyme, 1.5 μM RTRCVIA, 50 μM dansyl-GCVIA, and 5.0 μM [^{3}H]FPP. A 30-μL portion was removed and analyzed as described above. Blank reactions were obtained by substitution of buffer in place of RTRCVIA in the pulse solution.

Pre-Steady-State Kinetic Experiments. The approach to steady-state and single turnover measurements were performed using a KinTek rapid mixing apparatus (Johnson, 1995). The sample, reaction, quench, and exit loop volumes were measured to within 1% with a solution of [^{14}C]-isopentenyl diphosphate (400 cpm/μL). Measurements were performed with a pre-equilibrated solution of PFTase/[^{3}H]-FPP in the first sample loop (14.5 μL) and RTRCVIA in the second sample loop (14.5 μL), all in 50 mM Tris reaction buffer (pH = 7) at 30.0 °C. Final sample concentrations after mixing were 5.0−10.0 μM [^{3}H]FPP (1000 μCi/μmol), 0.3−0.7 μM PFTase, and 50.0−100.0 μM RTRCVIA for the rapid quench experiments and 100 nM [^{3}H]FPP, 700 nM PFTase, and 3.0 or 6.0 μM RTRCVIA for the single turnover experiments. Reactions were quenched with 200 μL of 0.2 M HCl. The ejected liquid was collected in 13 × 70 mm glass tubes, which were silanized with SigmaCote (Sigma) and placed on ice. Under these conditions (pH 0.8), the farnesylated product was stable, and neutralization of the reaction mixture was not necessary. A 75.0-μL portion was removed, spotted on a 1.5 × 4.5 cm phosphocellulose strip, and analyzed as described for the normal assay (20 mL wash/strip). Blank reactions were performed in separate Eppendorf tubes with quench added to pre-equilibrated E·FPP before the addition of RTRCVIA.

Pre-Steady-State Trapping of Enzyme-Bound Substrates. The rapid mixing apparatus was used to trap enzyme-bound substrate. Pre-equilibrated [^{3}H]FPP (10 μM, 900 μCi/μmol) and PFTase (400 nM) were mixed with RTRCVIA (100 μM) in 50 mM Tris assay buffer at 30 °C and allowed to react for 10−200 ms before diluting the reaction mixture with 200 μL of 100 μM unlabeled FPP from the central syringe on the mixing machine. The total volume ejected from the machine for each time point was 240 μL, of which 29 μL was the reaction mixture volume. The final specific activity of the original [^{3}H]FPP was therefore diluted more than 100-fold. After ejection into 13 × 70 mm silanized glass tubes, the mixtures were swirled for 15 s to allow any labeled intermediates to react before the addition of 30 μL of 1.5 M HCl to stop the reaction. A portion of the reaction mixture (85 μL) was spotted on a 1.5 × 4.5 cm phosphocellulose strip and analyzed as described above. Blank reactions were performed in separate tubes with HCl quench added to pre-equilibrated E·FPP before cold FPP and RTRCVIA.

Calorimetry. Enthalpies of reaction (ΔH_{rxn}) were obtained from thermograms collected with a Calorimetry Sciences Corporation (Provo, UT) isothermal titration calorimeter. The cell was calibrated at 25 °C with an internal cell heater. The titrate was a solution containing enzyme and excess FPP. RTRCVIA was the titrant. The buffer used for calorimetry consisted of a 20 mM ACES, HEPES, PIPES, or Tris buffer, pH 7.0, containing 10 mM $MgCl_2$, 10 μM $ZnCl_2$, 5 mM DTT, and 0.04% dodecyl-β-D-maltoside. Titrate solutions were prepared in the appropriate calorimetry buffer by diluting

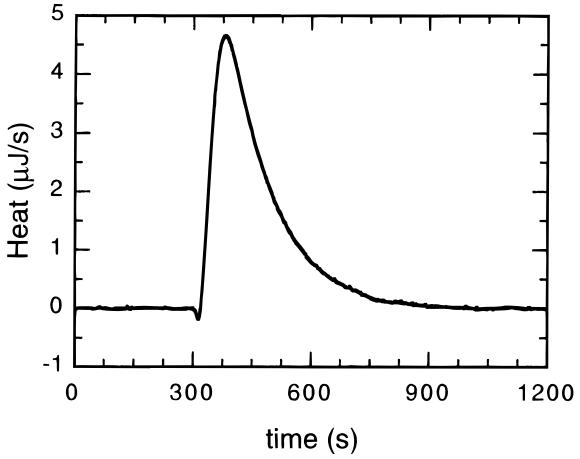

FIGURE 1: Thermogram (heat flow versus time) obtained for a single 10-μL injection of 1.74 mM RTRCVIA. The reaction cell contained 100 μM FPP and 200 nM PFTase in a total volume of 1.00 mL before injection. The small, endothermic dip at the initiation of titration represents the heat of dilution for peptide. The integrated area from 300 to 1000 s was 1182 μJ.

FPP and PFTase to concentrations of 100 μM and 200 nM, respectively, in a total volume of 1.40 mL. One milliliter of this mixture was transferred to the calorimeter cell using a glass syringe (Hamilton). The solution was allowed to equilibrate at 25 °C with stirring at 50 rpm for 30−45 min. A 100.0-μL glass syringe with an extended buret attachment was filled with 1.5−2.0 mM RTRCVIA in calorimetry buffer. The syringe was attached to the calorimeter with the buret tip immersed in the cell, and the system was allowed to equilibrate for an additional 5−10 min. A baseline signal was collected for at least 300 s before initiating the reaction with 5.0 or 10.0 μL of titrant. Heat output (μJ/s) was recorded every 0.5 s. Data for single titrations were collected for at least 1500 s. For sequential titrations, individual injections were spaced by 1200 s. Heats of dilution for titrants were obtained by an analogous procedure without enzyme in the reaction cell. Integration of the thermograms was performed with Kaleidagraph (Synergy Software, Reading, PA).

Numerical and Statistical Analysis. Kinetic constants were determined by a nonlinear regression fit of the coupled differential equations associated with the kinetic mechanism for PFTase to the pre-steady-state kinetic data. The standard error δk_i for each kinetic parameter k_i was obtained from the curvature of χ^2 with respect to k_i, and the propagation of errors formula was used to obtain standard errors for parameters calculated from fitted parameters (Bevington & Robinson, 1992). In some cases, kinetic constants were also determined by an explicit weighted nonlinear regression fit of the appropriate analytical expression utilizing Grafit (Erithicus Software, Staines, U.K.).

RESULTS

Enthalpy of Reaction for Farnesylation of Cysteine. Figure 1 shows a typical thermogram (heat flow versus time) obtained for a single 10-μL injection of 1.74 mM RTRCVIA into a reaction cell preloaded with 100 μM FPP and 200 nM PFTase in 1.0 mL total volume (before injection) of 20 mM PIPES buffer. The concentration of RTRCVIA was approximately 5-fold lower than that of FPP. The positive heat flow from the calorimeter cell quickly reached a

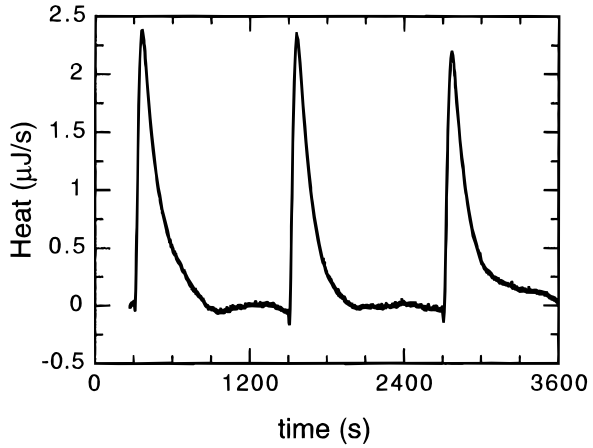

FIGURE 2: Thermogram for successive titrations. Substrate and enzyme concentrations were the same as in Figure 1. Each peak corresponds to the heat evolved after injection of 5 μL of 1.74 mM RTRCVIA. Integrated peak areas were (in sequence) 631, 530, and 638 μJ.

maximum after addition of the titrant and then decayed to baseline as the limiting substrate was depleted. The small, endothermic dip at the initiation of titration corresponded to the heat of dilution for peptide. Typical values obtained from identical experiments without enzyme were 3−4 μJ/μL of titrant. The integrated area from 300 to 1000 s in Figure 1 corresponded to 1182 μJ after correcting for the heat of dilution of peptide. The average integrated heat for six additional measurements (data not shown) was 1187 ± 70 μJ. Although kinetic information can be obtained from thermograms (Sturtevant, 1955; Morin & Freire, 1991; Williams & Toone, 1993), the response time of our calorimeter was not measured, and the apparent time required for the reactions shown in Figure 1 to proceed to completion was substantially longer than the actual time.

At constant temperature and pressure, the measured heat (Q) is directly proportional to the amount of product (P) formed and the enthalpy of reaction (ΔH_{rxn}) according to

$$dQ = dP\Delta H_{rxn}V_0 \quad (1)$$

where V_0 is the final cell volume after addition of the titrant (Tinoco et al., 1995; Wiseman et al., 1989). To determine ΔH_{rxn} from eq 1, the reaction must be functionally irreversible. This was confirmed for the PFTase reaction by conducting a sequence of titrations on the same solution of titrate. The thermogram from this experiment is shown in Figure 2. Substrate and enzyme concentrations were the same as for the experiment described in Figure 1. After measuring the baseline for 300 s, heat evolution was measured continuously for three 5-μL injections of 1.74 mM RTRCVIA spaced 1200 s apart. After correcting for the heat of dilution, the integrated areas for the three signals in Figure 2 were (in sequence) 631, 530, and 638 μJ. Additional titrations (data not shown) confirmed that on average each peak had the same area. If the reaction were partially reversible, the integrated heat signal should decrease with each additional titration because the starting concentration of FPP relative to the peptide also decreases. This relative change will shift the equilibrium by a small but detectable amount to give progressively less product and, as a consequence, a smaller evolution of heat in each cycle. All of the peptide injected during each titration apparently reacted

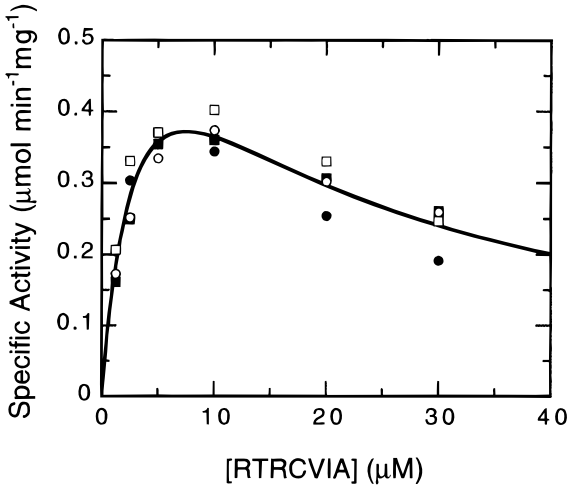

FIGURE 3: Plot of initial velocity versus the concentration of RTRCVIA containing 50 mM PIPES (○), HEPES (●), ACES (□) and Tris (■) assay buffers with 10 μM FPP and 2 nM PFTase. The fitted curve was obtained from eq 2 with $V = 0.72$ μmol min^{-1} mg^{-1}, $K_M^{PEP} = 3.5$ μM, and $K_I' = 16$ μM.

Scheme 2: Ordered Bireactant Mechanism with Inhibition by Peptide Substrate

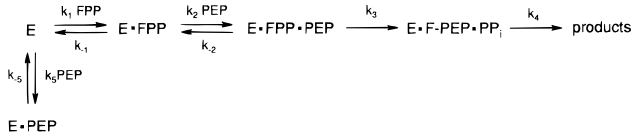

to form farnesylated RTRCVIA. The average value of ΔH_{rxn} for the farnesylation of cysteine from a total of eight measurements was −17 ± 1 kcal/mol.

Based on the pK_a values for inorganic pyrophosphate (PP_i), one would predict that the reaction should proceed with the net transfer of the sulfhydryl proton to PP_i in a pH 7 buffer. A potential source of error in the value for ΔH_{rxn} might arise from contributions to the measured enthalpy from protonation or deprotonation of the buffer. As a control, a series of successive titrations were conducted in 20 mM PIPES, HEPES, ACES, and Tris buffers (data not shown). Enthalpies of protonation (ΔH_{prot}) are −2.9, −5.2, −7.5 and −11.4 kcal/mol, for PIPES, HEPES, ACES, and Tris, respectively (Morin & Freire, 1991; Roig et al., 1993; Murphy et al., 1993), and represent a sufficiently large range to detect variations in ΔH_{rxn} due to net proton transfers to or from the buffer. Substrate and enzyme concentrations were the same for each experiment (100 μM FPP and 200 nM PFTase as the titrate, 5.0 μL of 1.66 mM RTRCVIA titrant). Integration of the thermograms obtained for each buffer showed no significant variation in calculated values for ΔH_{rxn}.

Initial Velocity Measurements. A minimal mechanism for the ordered addition of substrates by PFTase (Dolence et al., 1995) is shown in Scheme 2, where PEP represents RTRCVIA and F-PEP the farnesylated peptide. A control experiment using the filter paper assay was conducted to determine if RTRCVIA showed substrate inhibition, similar to that seen for dansyl-GCVIA in the fluorescence assay (Cassidy et al., 1995). A plot of initial velocities versus [RTRCVIA] measured in 50 mM Tris, HEPES, PIPES, and ACES assay buffers containing 10 μM FPP and 2 nM PFTase are shown in Figure 3. In each case, substrate inhibition was seen at higher concentrations of peptide. Furthermore,

the choice of buffer did not alter the inhibition pattern. A fit of the equation for substrate inhibition to the initial velocity, v, in Figure 3

$$v = \frac{V[\mathrm{PEP}]}{K_M^{\mathrm{PEP}} + [\mathrm{PEP}](1 + [\mathrm{PEP}]/K_I')} \qquad (2)$$

gave $V = 0.72$ μmol min^{-1} mg^{-1} ($k_{cat} = 1.0$ s^{-1}), $K_M^{PEP} = 3.5$ μM, and $K_I' = 16$ μM. In comparison, dansyl-GCVIA gave $V = 3.3$ μmol min^{-1} mg^{-1}, $K_M^{PEP} = 1.5$ μM, and $K_I' = 1.1$ μM at similar enzyme and substrate concentrations using a spectrofluorimetric assay (Dolence et al., 1995).

Initial velocity measurements were performed in duplicate for four concentrations of FPP (1.5−10.0 μM) and six concentrations of RTRCVIA (0.5−20.0 μM). Efforts to globally fit the two-dimensional steady-state rate equation associated with Scheme 2 (Dolence et al., 1995) to these data to were unsatisfactory. The higher concentrations of RTRCVIA needed to accurately determine the Michaelis constant for FPP (K_M^{FPP}) also produced substrate inhibition. A similar problem was observed with dansyl-GCVIA. Estimates for k_{cat}, K_M^{PEP}, and K_I for RTRCVIA were obtained graphically (Segal, 1975). Values were $k_{cat} = 1 \pm 1$ s^{-1}, $K_M^{PEP} = 2 \pm 1$ μM, and $K_I = 8 \pm 5$ μM.

Pulse−Chase Experiments. In the typical protocol for isotope trapping with a bireactant enzyme, labeled substrate is incubated with enzyme to form an E·S complex. The solution is then rapidly mixed with a second solution containing the second substrate and a large excess (>100-fold) of unlabeled first substrate (Rose, 1980). Upon mixing the two solutions, labeled first substrate that dissociates from the E·S complex before it is converted to product is trapped by the higher concentration of unlabeled substrate, and its specific activity is reduced to a negligible level. The amount of label in the product reflects the amount of E·S that is converted to product before dissociation to E + S.

As a variation on this strategy, we used a trifluorinated derivative of FPP (TFPP) in place of unlabeled FPP in the chase solution to trap E·FPP. The fluorinated analog was much less reactive (770-fold) and bound more tightly (5-fold) than FPP to PFTase (Dolence & Poulter, 1995; Dolence et al., 1995). Thus, TFPP served as a more efficient trapping reagent. Using the partition approach of Cleland (1975), the amount of radioactivity appearing in the observed product (F-PEP$_{obs}$) is

$$[\text{F-PEP}_{obs}] = \frac{\text{E·FPP}_0[\mathrm{PEP}]}{K_{1/2} + [\mathrm{PEP}]} \qquad K_{1/2} = k_{-1}\left(\frac{k_{-2} + k_3}{k_2 k_3}\right) \qquad (3)$$

where E·FPP$_0$ is the concentration of enzyme-bound FPP, $K_{1/2}$ is the peptide concentration needed to convert half of the E·FPP complex to product, and PEP is the concentration of peptide after mixing the pulse and chase solutions. The results are shown in Figure 4. A fit of eq 3 to the data yielded $K_{1/2} = 0.57 \pm 0.03$ μM. The fitted value for [E·FPP$_0$] (88 ± 4 nM) was similar to the value calculated from K_D^{FPP} and the enzyme and substrate concentrations used in the experiment, suggesting that enzyme-bound FPP was efficiently trapped and was converted to product irreversibly. The experiment was repeated twice with similar results.

Trapping of enzyme-bound RTRCVIA was also attempted. Control experiments showed that [^{3}H]farnesylated dansyl-GCVIA was not retained on the filter paper after workup. Thus, dansyl-GCVIA, an alternate peptide substrate, served as a suitable chase reagent. Enzyme and RTRCVIA were mixed to form the pulse solution, and dansyl-GCVIA and [^{3}H]FPP were combined for the chase. At the highest concentrations of FPP (67 × K_D^{FPP} and 10 × K_M^{FPP}) used in the chase, less than 3% of the starting RTRCVIA was converted to product under these conditions. Since the concentration of [^{3}H]FPP used in the experiment was nearly 10-fold larger than the value of $K_{1/2}$ determined from Figure 4, the principle route to a catalytically active ternary complex involved the addition of FPP before peptide. This conclusion agrees with previous steady-state kinetic studies with yeast PFTase (Dolence et al., 1995).

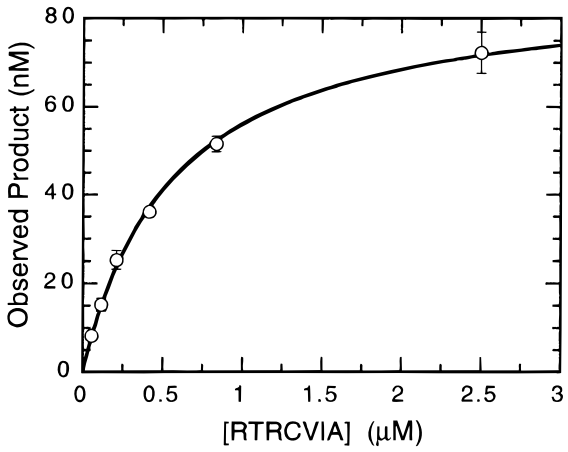

FIGURE 4: Plot of enzyme-bound [^{3}H]FPP that is converted to product versus the concentration of RTRCVIA. The error bars refer to ranges of duplicate determinations. The pulse solutions contained 1.4 μM PFTase and 200 nM [^{3}H]FPP in 50 mM Tris reaction buffer. Since $K_D^{FPP} = 75 \pm 15$ nM (Dolence et al., 1995), greater than 90% of the [^{3}H]FPP was bound. The chase solutions contained 0.1−5.0 μM RTRCVIA and 70 μM TFPP. Concentrations were diluted 2-fold upon mixing of the pulse and chase solutions. The displayed curve was obtained from eq 3 with $K_{1/2} = 0.57 \pm 0.03$ μM and E·FPP$_0$ = 88 ± 4 nM.

Rapid Quench Experiments. Rapid quench techniques were used for pre-steady-state kinetic measurements (Fersht, 1985; Anderson et al., 1988; Johnson, 1995; Fierke & Hammes, 1995). The efficiency of the HCl quench was determined for various concentrations of the acid. Duplicate measurements spaced 5−10 min apart, but worked up consecutively, were in agreement if HCl concentrations were greater than 50 mM. Figure 5 shows a plot for the formation of product from 5 to 500 ms for 5 μM [^{3}H]FPP, 50 μM RTRCVIA, and 350 nM PFTase. The error bars represent the range of duplicate determinations. The burst amplitude is small, which indicates that *both* the chemical and the product release steps are important in determining k_{cat}.

Scheme 3 shows the minimal mechanism used to interpret the rapid quench results. Binding of FPP to free enzyme after the first turnover was assumed to be fast as compared to peptide binding and catalysis (see below). The formation of product as a function of reaction time t is given by eq 4 (Fersht, 1985; Fierke & Hammes, 1995)

$$[\text{F-PEP}_{obs}] = [\text{F-PEP}] + [\text{E·F-PEP·PP}_i] = \alpha[1 - e^{-\beta t}] + \gamma t \qquad (4)$$

where α is the apparent burst amplitude, β is the reciprocal

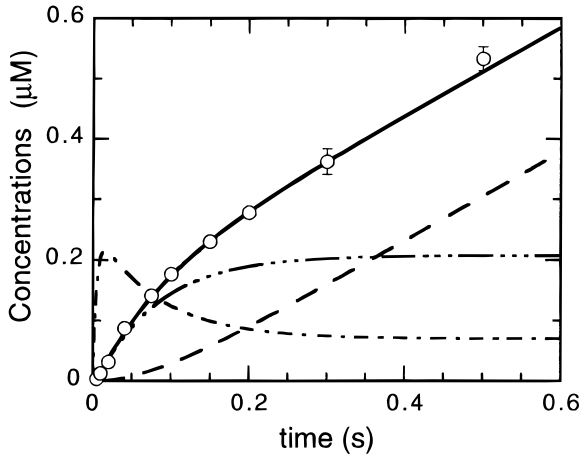

FIGURE 5: Plot of the formation of farnesylated RTRCVIA between 5 and 500 ms. Enzyme and substrate concentrations were 5 μM [^{3}H]FPP, 50 μM RTRCVIA, and 350 nM PFTase. The error bars represent the range of duplicate determinations. The progress curves for intermediates E·FPP·PEP (—·—) and E·F-PEP·PP$_i$ (—···—), and product F-PEP (---) were calculated by integration of the differential equations associated with Scheme 3 using the rate constants in Table 1 and reactant and enzyme concentrations listed above. The solid line (—) corresponds to the sum of E·F-PEP·PP$_i$ and F-PEP.

Scheme 3: Mechanism for Conversion of Binary E·FPP Complex to Products

$$\text{E·FPP} \underset{k_{-2}}{\overset{k_2\,\text{PEP}}{\rightleftharpoons}} \text{E·FPP·PEP} \xrightarrow{k_3} \text{E·F-PEP·PP}_i \xrightarrow{k_4} \text{products}$$

lifetime of E·F-PEP·PP$_i$, γ is the steady-state rate

$$\alpha = \text{E·FPP}_0\left(\frac{k'}{k' + k_4}\right)^2 \qquad \beta = k' + k_4$$

$$\gamma = \text{E·FPP}_0\left(\frac{k'k_4}{k' + k_4}\right) \quad (5)$$

and k' is the effective first-order rate constant for formation of E·F-PEP·PP$_i$:

$$k' = \frac{k_3[\text{PEP}]}{(k_{-2} + k_3)/k_2 + [\text{PEP}]} \quad (6)$$

The derivation of eq 4 invokes a steady-state approximation for the concentration of the ternary reactant complex (E·FPP·PEP) and assumes that the time derivative of PEP is zero (dPEP/dt = 0) in order to linearize the coupled differential equations and permit an analytic solution. A fit of eq 4 to the data in Figure 5 yielded $\alpha = 0.13 \pm 0.03$ μM, $\beta = 12 \pm 3.0$ s^{-1}, and $\gamma = 0.82 \pm 0.06$ μM s^{-1}. Since the experiment was conducted with a high concentration of RTRCVIA, k' in eq 6 was approximately equal to k_3. With this approximation, rearrangement of eq 5 and application of the propagation of errors formula yielded $k_3 = 8.0 \pm 3.2$ s^{-1}, $k_4 = 4.2 \pm 1.1$ s^{-1}, and E·FPP$_0 = 0.30 \pm 0.06$ μM. The enzyme concentration employed in the experiment (determined by UV absorption) was 0.35 μM, in agreement with the fitted value. Note that the apparent burst amplitude (0.13 μM) was significantly smaller than the employed enzyme concentration, due to the similarity of k_3 and k_4. Variations of substrate and enzyme concentrations (50−100 μM RTRCVIA, 5−10 μM FPP, 0.2−0.8 μM PFTase) and the time interval over which the reaction was monitored (up to 2 s) did not significantly change the value for β (data not shown). Since the tritium label of [^{3}H]FPP was at C1, the value for k_3 may include an α secondary isotope effect. However, recent studies for a related allylic system, the chorismate synthase-catalyzed formation of chorismate from 5-enolpyruvylshikimate 3-phosphate suggests that the magnitude of the isotope effect will be less than 10% (Balasubramanian et al., 1995).

In order to assess the effect of substrate inhibition, time curves were obtained by combining preformed E·FPP with RTRCVIA and by combining free enzyme with a mixture of FPP and RTRCVIA. Final concentrations after mixing for both experiments were 50 μM RTRCVIA, 5 μM [^{3}H]-FPP, and 200 nM PFTase. Time curves measured from 40 to 500 ms, corresponding to three enzyme turnovers, had the same apparent burst amplitude and steady-state rate. Since substrate inhibition reduces the concentration of free enzyme available for catalysis, the time curve for preformed E·FPP should have shown a larger apparent burst amplitude and steady-state rate as compared to the time curve for free enzyme if substrate inhibition was an important factor in our rapid quench experiments. Our results indicated that PEP did not substantially alter the amount of free enzyme available for binding FPP for the concentrations of enzyme and substrates used in the rapid quench experiments. These observations support the use of the simplified Scheme 3 to model the rapid quench kinetics.

Pre-Steady-State Isotope Trapping Experiments. A set of isotope trapping experiments using cold FPP was performed with the rapid mixing apparatus. Each experiment was run in parallel with an HCl quench. PFTase and [^{3}H]FPP were preincubated before mixing with peptide to a final concentration of 200 nM enzyme, 5 μM [^{3}H]FPP, and 50 μM RTRCVIA. After a specified time interval, the reaction was quenched with 100 μM cold FPP and allowed to incubate for 15 s before the addition of HCl to a final concentration of 0.17 M. When HCl was used in the quench, the acid immediately inactivated PFTase and the radioactivity in farnesylated RTRCVIA represented the sum of free F-PEP and E·F-PEP. In contrast, FPP did not inactivate the enzyme. Thus, the radioactivity in the farnesylated peptide in an FPP trap was the sum of F-PEP, E·F-PEP, E·FPP·PEP, and the fraction of E·FPP that was committed to catalysis. The 15-s interval between the addition of cold FPP and the addition of HCl was sufficient for all of the ternary complex to turnover, and the 200-fold dilution of radioactivity in FPP was sufficient to supress additional formation of [^{3}H]F-PEP from free enzyme.

The results for addition of cold FPP (open circles) and HCl (closed circles) are shown in Figure 6a. The time course for the HCl quench was similar to that shown in Figure 5. However, the time course for isotope trapping by cold FPP was constant at reaction times corresponding to the first turnover of E·FPP and then increaseed in parallel with the HCl curve. The amount of product formed at short reaction times closely corresponded to the amount of enzyme used in the reaction. These results indicate that FPP is a "sticky" substrate and that the E·FPP complex is efficiently converted to product in the presence of peptide.

A difference plot for the two time courses (see Figure 6b) corresponds to the sum of the time courses for E·FPP and E·FPP·PEP. The time scale for conversion of E·FPP to E·FPP·PEP was fast under the conditions of the experiment ([RTRCVIA] = 15 × K_M^{PEP}) and the data in Figure 6b

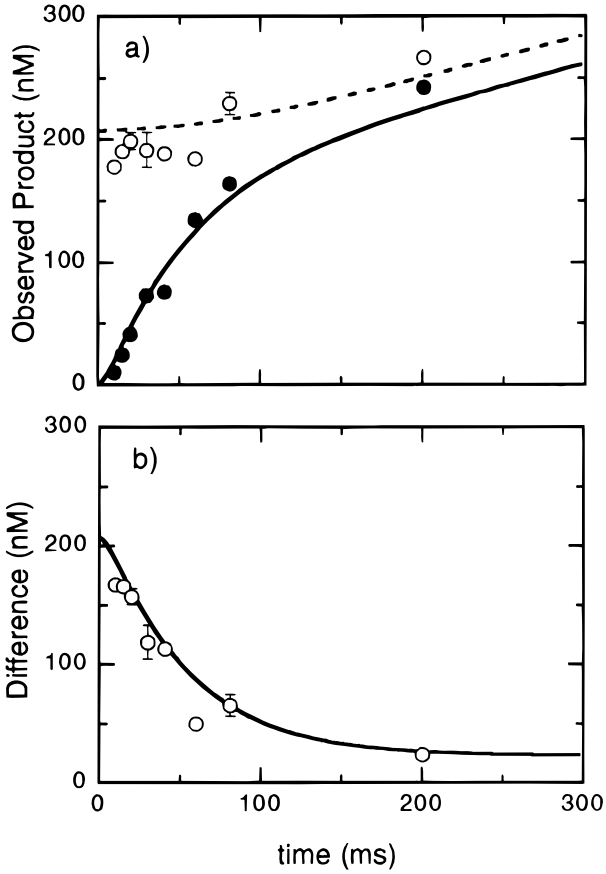

FIGURE 6: Time course for formation of radiolabeled peptide. An isotope trapping experiment performed with the rapid mixing machine. (a) Time courses obtained with HCl quench (●) and 100 μM cold FPP dilution (○). The enzyme concentration was 200 nM, and substrate concentrations were 5 μM [^{3}H]FPP and 50 μM RTRCVIA. The reaction was quenched by the addition of HCl or cold FPP. The error bars for the open data points represent the scatter observed with duplicate determinations. The theoretical curves were generated with the rate constants in Table 1 and the enzyme and substrate concentrations listed above. (b) Difference between the 100 μM cold FPP data points and the HCl data points, corresponding to the time dependence of E·FPP + E·FPP·PEP. The displayed line is the theoretical time dependence of E·FPP + E·FPP·PEP.

primarily represent the conversion of the ternary reactant complex to product. The expression for the time dependence of E·FPP·PEP is given by

$$[\text{E·FPP·PEP}] = a + be^{-\beta t} \qquad (7)$$

where a is approximately the steady-state concentration of E·FPP·PEP, b is proportional to the enzyme concentration, and β is the decay constant given in eq 5. A fit of eq 7 to the data in Figure 6b gave $a = 20 \pm 15$ nM, $b = 181 \pm 15$ nM, and $\beta = 16 \pm 4$ s^{-1}. This value for β compares well with the value for β obtained from eq 4 and Figure 5 (12 ± 3 s^{-1}). Interpretation of the values for a and b is difficult because of the approximations associated with eq 7.

Additional experiments using 10−50 μM TFPP or 100 mM EDTA in place of 100 μM cold FPP were also performed (data not shown). Since TFPP was a competitive inhibitor of PFTase with respect to FPP and noncompetitive with respect to peptide (Dolence et al., 1995), the fluorinated analog stopped the reaction by binding to free enzyme following turnover. EDTA quenched the reaction by complexing with Mg^{2+}, a necessary metal for productive binding

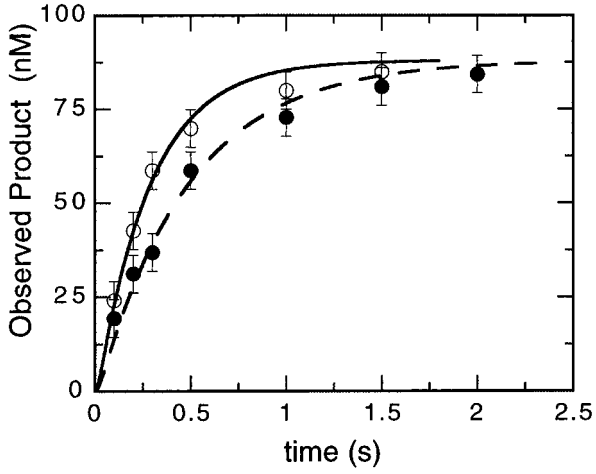

FIGURE 7: Plot of the pseudo-first-order appearance of product associated with a single turnover of enzyme-bound FPP. Concentrations before addition of the quench were 700 nM PFTase, 100 nM [^{3}H]FPP, and 3 (●) or 6 (○) μM RTRCVIA. Fits of eq 8 yielded $k' = 2.2 \pm 0.2$ and 3.9 ± 0.3 s^{-1} for 3 and 6 μM RTRCVIA, respectively. The fitted value for E·FPP$_0$ was 90 ± 5 nM for both experiments. The curves are theoretical observed product (E·F-PEP·PP$_i$ + F-PEP) concentrations as a function of time, calculated by integration of the differential equations associated with Scheme 3 using the rate constants in Table 1 and reactant and enzyme concentrations listed above.

of FPP. Both of these reagents gave results similar to those obtained for cold FPP (data not shown).

Single Turnover Experiments. Kinetic measurements for a single turnover of enzyme-bound FPP were conducted by mixing a pre-equilibrated solution of 700 nM PFTase and 100 nM [^{3}H]FPP with 3 or 6 μM RTRCVIA. Under these conditions, greater than 90% of the [^{3}H]FPP was bound (Dolence et al., 1995). The results are displayed in Figure 7. The reactions were quenched with 0.2 M HCl, and radioactivity in the product was measured by the strip assay. A plot of F-PEP versus time appeared to follow first-order kinetics (Figure 7).

The equation for pseudo-first-order formation of product is given by

$$[\text{F-PEP}_{\text{obs}}] = \text{E·FPP}_0(1 - e^{-k't}) \qquad (8)$$

where k' is the same as in eq 6. As seen for eq 4, eq 8 assumes that [PEP] ≫ [E·FPP] and that E·FPP·PEP is at steady state. Fits of eq 8 to the data in Figure 7 gave values for k' of 2.2 ± 0.2 and 3.9 ± 0.3 s^{-1} for 3 and 6 μM RTRCVIA, respectively. The net rate constant for peptide binding, given by

$$k_{\text{net}} = k_2\left(\frac{k_3}{k_{-2} + k_3}\right) \approx k'/[\text{RTRCVIA}] \qquad (9)$$

was 7×10^5 M^{-1} s^{-1}. The fitted value for E·FPP$_0 = 90 \pm 5$ nM for both fits agreed with the concentrations used in the experiments.

Evaluation of Rate Constants. The values for constants obtained from Figures 4, 5, and 7 ($K_{1/2}$, k_3, k_4, k_{net}) and the value for $K_D^{\text{FPP}} = 75$ nM (Dolence et al., 1995) constitute five of the six unique parameters necessary to evaluate the individual rate constants ($k_{\pm1}$, $k_{\pm2}$, k_3, k_4) defined in Scheme 2. The value for the peptide dissociation constant, $K_D^{\text{PEP}} =$

Table 1: Individual Kinetic Constants for Farnesylation of RTRCVIA Catalyzed by Yeast PFTase[a] and Calculated Values for the Associated Michaelis and Dissociation Constants[b]

k_1[c]	$6.4 \pm 1.4 \times 10^6$ M^{-1} s^{-1}	k_{cat}	2.6 ± 0.1 s^{-1}	$(1 \pm 1$ s$^{-1})$[d]
k_{-1}[c]	0.48 ± 0.04 s^{-1}	K_M^{FPP}	420 ± 90 nM	
k_2	$3.5 \pm 0.2 \times 10^6$ M^{-1} s^{-1}	K_D^{FPP}		$(75 \pm 15$ nM)[e]
k_{-2}	33 ± 2 s^{-1}	K_M^{PEP}	3.1 ± 0.2 μM	$(2 \pm 1$ μM)[d]
k_3	10.5 ± 0.1 s^{-1}	K_D^{PEP}	9.5 ± 0.6 μM	
k_4	3.5 ± 0.2 s^{-1}	k_{net}	$8.4 \pm 0.5 \times 10^5$ M^{-1} s^{-1}	

[a] $k_{\pm 2}$, k_3, and k_4 obtained from a fit to the differential equations associated with Schemes 2 and 3 (see Figure 8). [b] Steady-state kinetic constants and dissociation constants were calculated from individual rate constants using eqs 9−12. [c] Obtained from the measured value of $K_{1/2} = 0.57$ μM (Figure 4) and K_D^{FPP}. [d] Measured values (see discussion below eq 2). [e] Measured by equilibrium dialysis (Dolence et al., 1995).

k_{-2}/k_2, for the ternary E·FPP·PEP would permit us to complete the evaluation of the individual kinetic constants. A direct measurement of K_D^{PEP} was not possible under normal catalytic conditions, and replacement of FPP with an inactive analog may alter the binding of the peptide substrate. We obtained an estimate of K_D^{PEP} by a nonlinear regression fit of the numerically integrated coupled differential equations associated with Scheme 3 to the rapid quench and single turnover data in Figures 5 and 7. The fit varied the four rate constants $k_{\pm 2}$, k_3, and k_4 independently. Concentrations were expressed as micromolar, and time was in seconds. Enzyme and substrate concentrations were not treated as variables and were fixed at their experimental values. Final values for these four rate constants were then combined with $K_{1/2}$ and K_D^{FPP} to calculate values for k_1 and k_{-1}. Recall that the steady-state approximation for E·FPP·PEP was made in eqs 4 and 8, and that dPEP/dt was ignored. Numerical integration makes no approximations regarding the time dependence of the concentrations of species undergoing reaction. All of the rapid quench kinetic data were combined and fit simultaneously.

The FORTRAN code written to perform the analysis employed a fourth-order Runge−Kutta numerical integration subroutine (Press et al., 1992) to integrate the differential equations (dE/dt, dFPP/dt, etc.) associated with the mechanism shown in Scheme 3 for each trial set of rate constants. A nonlinear least squares subroutine (Chandler, 1976) linked to the integration routine varied the rate constants and made repeated calls to the integration routine until a global minimum in χ^2 was found. χ^2 is defined by

$$\chi^2 = \sum_i \left\{ \frac{y_i - y(x_i)}{\sigma_i} \right\}^2 \qquad (10)$$

where y_i is the observed product concentration for data point i, $y(x_i)$ is the calculated value, and σ_i is the experimental error. When a global minimum of χ^2 was found, output files were generated that contained (1) best fits for the rate constants, (2) values for χ^2 calculated over a ±50% range for each k_i holding the other rate constants fixed at their best fitted values, and (3) theoretical time course curves for direct comparisons with experimental data. A time step of 0.1 ms was sufficient to ensure conservation of enzyme or limiting substrate to one part in 10^5. A typical run required approximately 500 iterations, and calculation of the final output required 2−3 min of real time on a Silicon Graphics Indigo2 workstation.

Results for fitting the mechanism in Scheme 3 to the data in Figures 5 and 7 are presented in Table 1. Random variations of the starting values for $k_{\pm 2}$, k_3, and k_4, such that χ^2 for the first fitting iteration was 10^3−10^4-fold larger than the global minimum, did not change the final values for the rate constants. To produce such large initial values for χ^2 for the first iteration, starting values for rate constants of up to ±3 orders of magnitude different than the final fitted values were used in over 50 different runs, all of which converged to the same values. Figure 8 shows the behavior of χ^2 versus each rate constant holding the others fixed at their respective best fit values, in effect showing two-dimensional projections of the $\chi^2(k_2, k_{-2}, k_3, k_4)$ hypersurface in the neighborhood of the global minimum. The abscissa in Figure 8 was normalized to account for differences in units and magnitudes between the rate constants and displays a 50% variation for each parameter. The ordinate was scaled by the minimum value of χ^2. An increase in χ^2 by a factor of 5 or more for a 50% change in parameter provided a measure of the quality of the fit. The standard error, δk_i, for each k_i was obtained from the inverse curvature of $\chi^2(k_i)$ evaluated at the minimum (Bevington & Robinson, 1992). The curvature of the χ^2 projection for k_3 in Figure 8 was particularly large and translated into a standard error of less than 1% for this rate constant. Standard errors for the remaining rate constants (k_2, k_{-2}, and k_4) were approximately 6%. Inclusion of the pre-steady-state isotope trapping data in Figure 6, performed with a different batch of enzyme, resulted in similar fitted values for rate constants but increased the standard errors to ±20−30%. While all fitting procedures are subject to artifacts arising from local minima, we feel that this possibility was minimized by the large range of starting conditions we explored.

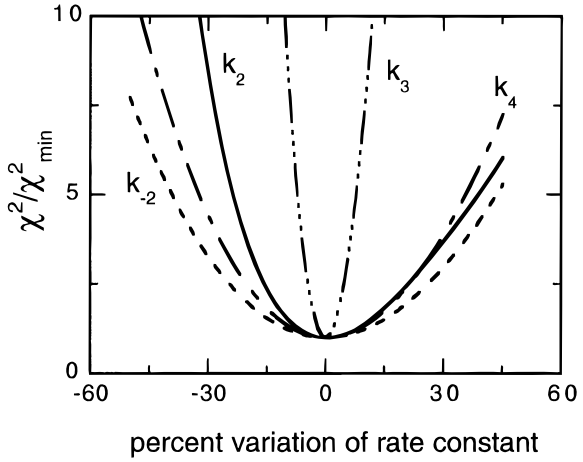

FIGURE 8: Two-dimensional projections of the $\chi^2(k_2, k_{-2}, k_3, k_4)$ hypersurface in the vicinity of the global minimum. Each curve represents the variation of χ^2 (see eq 10) with respect to the rate constant labeled near the curve holding the remaining three fixed and equal to their best fit values (Table 1). The abscissa was scaled according to $(k/k_{min} - 1) \times 100\%$ to account for differences in units and magnitudes. The ordinate was scaled by χ^2_{min}, the minimized value for χ^2.

Using fitted values for $k_{\pm 2}$ and k_3, the FPP binding (k_1) and dissociation (k_{-1}) rate constants were evaluated from $K_{1/2}$ and K_D^{FPP}. k_{-1} is related to k_{net} and $K_{1/2}$ according to

$$k_{-1} = k_{net}K_{1/2} \quad (11)$$

For $K_{1/2} = 0.57 \pm 0.03$ μM and $k_{net} = 0.84 \pm 0.05 \times 10^6$ M^{-1} s^{-1} calculated from the fitted rate constants in Table 1, $k_{-1} = 0.48 \pm 0.04$ s^{-1}. $k_1 = 6.4 \pm 1.4 \times 10^6$ M^{-1} s^{-1} was obtained from k_{-1} and $K_D^{FPP} = k_{-1}/k_1 = 75 \pm 15$ nM.

The steady-state parameters k_{cat}, K_M^{FPP}, and K_M^{PEP} were calculated according to

$$k_{cat} = \frac{k_3k_4}{k_3 + k_4} \qquad K_M^{FPP} = \frac{k_3k_4}{k_1(k_3 + k_4)}$$

$$K_M^{PEP} = \frac{k_4(k_{-2} + k_3)}{k_2(k_3 + k_4)} \quad (12)$$

The values were $k_{cat} = 2.6 \pm 0.1$ s^{-1}, $K_M^{FPP} = 420 \pm 90$ nM, and $K_M^{PEP} = 3.1 \pm 0.2$ μM. k_{cat} and K_M^{PEP} obtained from eq 12 were similar to those obtained from the steady-state measurements (see above).

An inspection of the kinetic and binding constants in Table 1 shows that the dissociation constant for FPP (K_D^{FPP}) was nearly 5-fold smaller than its Michaelis constant. This indicates that when FPP binds to PFTase there is a 5-fold larger probability of reaction as compared to dissociation i.e., there is a high commitment to catalysis. For the peptide dissociation constant, the ratio of k_{-2} and k_2 gave $K_D^{PEP} = 9.5 \pm 0.6$ μM, which was similar to the steady-state inhibition constant $K_I = 8$ μM. In contrast to FPP, the peptide dissociation constant was 3-fold *larger* than its Michaelis constant, consistent with an accumulation of enzyme-bound intermediates after the peptide binding step. This is expected when product release is slower than conversion of enzyme-bound substrate to enzyme-bound product (Fersht, 1985).

Figure 5 shows theoretical progress curves for intermediates (E·FPP·PEP and E·F-PEP·PP_i) and free F-PEP calculated from the rate constants listed in Table 1. The amount of product (F-PEP_{obs}) observed in the single turnover experiments is the sum of E·F-PEP·PP_i and F-PEP. The simulated curves for F-PEP_{obs} shown in Figures 6 and 7 were also calculated using the rate constants in Table 1 and the enzyme and substrate concentrations used in each experiment. Note that the simulated concentrations of intermediates in Figure 5 approach their steady-state values after 200 ms. Of the 23 data points used for the differential equation fit (10 from Figure 5, 13 from Figure 7), nine were measured at $t < 200$ ms.

DISCUSSION

PFTase, PGGTase-I, and PGGTase II are related at the structural and the functional level. All three enzymes are heterodimers with a substantial degree of amino acid sequence similarity, and all are Zn^{2+} metalloproteins. Although the three prenyltransferases have different selectivities for their isoprenoid and protein substrates, each catalyzes a nucleophilic substitution of the diphosphate moiety in their allylic isoprenoid substrates by the sulfhydryl group in cysteine. Work with PFTase shows that the reaction proceeds with inversion of configuration (Mu et al., 1996). Inhibition studies with transition-state analogs (Cassidy & Poulter, 1996) and linear free energy correlations with fluorinated analogs of FPP (Dolence & Poulter, 1995) indicate that the reaction proceeds by an enforced mechanism through an exploded, highly polar transition state.

PFTase and PGGTase I bind substrates by an ordered mechanism. Although the results of steady-state studies were ambiguous for the mammalian enzymes (Pompliano et al., 1992, 1993), their yeast counterparts gave classic double-reciprocal profiles for an ordered binding mechanism where the isoprenoid substrate adds first (Dolence et al., 1995). Isotope trapping experiments performed with the mammalian enzyme, however, clearly indicated that the isoprenoid diphosphate added before protein or peptide by an ordered process (Furfine et al., 1995). Under normal catalytic conditions, the prenylation of cysteine is irreversible, and thus, the order in which products are released has not been determined.

The enthalpy we measured for farnesylation of cysteine in RTRCVIA by FPP in pH 7 buffer was large and exothermic ($\Delta H_{rxn} = -17$ kcal/mol), consistent with an irreversible chemical step in the enzyme-catalyzed reaction. This value is 5 kcal/mol less exothermic than the estimate of -22 kcal/mol, obtained from average SH (90), CO (82), OH (119), and CS (75) gas-phase bond enthalpies (Griller et al., 1988). The rough agreement between the measured and estimated enthalpies of reaction evidently arises from a cancellation of errors associated with enthalpies of solvation.

In the present work, the combination of data obtained from pre-steady-state, isotope partitioning, and equilibrium dialysis experiments was sufficient to determine all of the rate constants associated with the farnesylation of RTRCVIA. Rate constants for peptide binding, conversion to product, and product release were deduced from rapid quench and single turnover measurements by performing a nonlinear regression fit of the differential equations associated with Scheme 3. The FORTRAN program written to perform the fit employed an accurate, variable step fourth-order Runge−Kutta numerical integration routine, which was coupled to a nonlinear least squares fitting routine based on the Marqardt algorithm (Press et al., 1992; Chandler, 1976). Both of these program components are well-documented, freely available routines that are aptly suited for the fitting of time curves based on simulation. One aspect distinguishing our program from others discussed in the literature (Zimmerle & Frieden, 1989; Holzhütter & Colosimo, 1990) is the graphic generation of the χ^2 hypersurface (*cf.* eq 10 and Figure 8), thereby allowing both a visual inspection of the quality of the fit and a calculation of standard errors for each fitted parameter (Bevington & Robinson, 1992).

The individual rate constants listed in Table 1 provide a detailed profile for the step up to the release of products. The rates for the addition of FPP to free enzyme and the addition of peptide to the E·FPP complex are similar, and in the 10^6-10^7 M^{-1} s^{-1} range typical of protein−small molecule association rate constants for additions not limited by a conformational change in the protein. However, the off-rate for dissociation of peptide from the ternary E·FPP·PEP complex is 70-fold faster than for dissociation of FPP from the binary E·FPP complex. Thus, E·FPP can be efficiently trapped by added peptide and converted to product in spite of an unfavorable partitioning of the ternary complex between dissociation of peptide and conversion to product. The difference in dissociation rate constants is also manifest

in the substantially smaller dissociation constant for E·FPP than for E·FPP·PEP.

The catalytic constant for yeast PFTase ($k_{cat} = 2.6\ s^{-1}$) is 40 times larger than for the mammalian enzyme ($k_{cat} = 0.06\ s^{-1}$; Furfine et al., 1995). Although not all of the individual rate constants listed in Table 1. available for mammalian PFTase, the rate-limiting step for turnover is thought to be dissociation of the enzyme−product complex. For yeast PFTase, the chemical step (k_3) is only three times faster than product release (k_4). Given the observation that FPP and peptide bind more tightly to mammalian PFTase than its yeast counterpart, it is likely that the difference in k_{cat} for the two enzymes is determined by dissociation rather than chemistry.

In summary, yeast PFTase catalyzes the electrophilic alkylation of cysteine by FPP. Substrate addition is ordered with FPP being substantially more "sticky" than peptide. Turnover is limited by the rate of dissociation of the enzyme−product complex, although the overall rate for product release is only three times slower than the chemical step.

ACKNOWLEDGMENT

We thank Dr. Koji Ando for providing us a copy of the nonlinear least squares program component, Dr. Julia Dolence for a sample of 13-trifluoroFPP, and Daria Pori for her technical assistance.

REFERENCES

Anderson, K. S., Sikorski, J. A., & Johnson, K. A. (1988) *Biochemistry 27*, 7395.
Balasubramanian, S., Coggins, J. R., & Abell, C. (1995) *Biochemistry 34*, 341.
Bevington, P. R., & Robinson, D. K. (1992) *Data Reduction and Error Analysis for the Physical Sciences*, 2nd ed., McGraw-Hill, New York.
Bradford, M. M. (1976) *Anal. Biochem. 72*, 248.
Casey, P. J. (1994) *Curr. Opin. Cell. Biol. 6*, 219.
Cassidy, P. B., & Poulter, C. D. (1996) *J. Am Chem. Soc. 118*, 8761.
Cassidy, P. B., Dolence, J. M., & Poulter, C. D. (1995) *Methods Enzymol. 250*, 30.
Chandler, J. P. (1976) *Quant. Chem. Prog. Exp. 11*, 307.
Clarke, S. (1992) *Annu. Rev. Biochem. 61*, 355.
Cleland, W. W. (1975) *Biochemistry 14*, 3220.
Davisson, V. J., Woodside, A. B., Neal, T. R., Stremler, K. E., Muehlbacher, M., & Poulter, C. D. (1986) *J. Org. Chem. 51*, 4768.
Dolence, J. M., & Poulter, C. D. (1995) *Proc. Natl. Acad. Sci. U.S.A. 92*, 5008.
Dolence, J. M., Cassidy, P. B., Mathis, J. R., & Poulter, C. D. (1995) *Biochemistry 34*, 16687.
Fersht, A. (1985) *Enzyme Structure and Mechanism*, 2nd ed., W. H. Freeman and Co., New York.
Fierke, C. A., & Hammes, G. G. (1995) *Methods Enzymol. 249*, 3.
Furfine, E. S., Leban, J. J., Landavazo, A., Moomaw, J. F., & Casey, P. J. (1995) *Biochemistry 34*, 6857.
Goldstein, J. L., & Brown, M. S. (1990) *Nature 343*, 425.
Gomez, R., Goodman, L. E., Tripathy, S. K., O'Rourke, E., Manne, V., & Tamanoi, F. (1993) *Biochem. J. 289*, 25.
Gill, S. C., & von Hippel, P. H. (1989) *Anal. Biochem. 182*, 319.
Good, N. E., & Izawa, S. (1972) *Methods Enzymol. 24*, 53.
Griller, D., Kanabus-Kaminska, J. M., & Maccoll, A. (1988) *J. Mol. Struct. 163*, 125.
Holzhütter, H. G., & Colosimo, A. (1990) *Comput. Appl. Biosci. 6*, 23.
Johnson, K. A. (1986) *Methods Enzymol 134*, 677.
Johnson, K. A. (1995) *Methods Enzymol. 249*, 38.
Mayer, M. P., Prestwich, G. D., Dolence, J. M., Bond, P. D., Wu, H.-Y., & Poulter, C. D. (1993) *Gene 132*, 41.
Moores, S. L., Schaber, M. D., Mosser, S. D., Rands, E., O'Hara, M. B., Garsky, V. M., Marshall, M. S., Pompliano, D. L., & Gibbs, J. B.(1991) *J. Biol. Chem. 266*, 14603.
Morin, P. E., & Freire, E. (1991) *Biochemistry 30*, 8494.
Mu, Y.-Q., Omer, C. A., & Gibbs, R. A. (1996) *J. Am Chem. Soc.* 118, 1817.
Murphy, K. P., Xie, D., Garcia, K. C., Amzel, L. M., & Freire, E. (1993) *Proteins 15*, 113.
Omer, C. A., Kral, A. M., Diehl, R. E., Prendergast, G. C., Powers, S., Allen, C. M., Gibbs, J. B., & Kohl, N. E. (1993) *Biochemistry 32*, 5167.
Pompliano, D. L., Rands, E., Schaber, M. D., Mosser, S. D., Anthony, N. J., & Gibbs, J. B. (1992) *Biochemistry 31*, 3800.
Pompliano, D. L., Schaber, M. D., Mosser, S. D., Omer, C. A., Shafer, J. A., & Gibbs, J. B. (1993) *Biochemistry 32*, 8341.
Press, W. H., Vetterling, W. T., Teukolsky, S. A., & Flannery, B. P. (1992) *Numerical Recipies in Fortran*, 2nd. ed., Cambridge University Press, Cambridge.
Rando, R. R. (1996) *Biochim. Biophys. Acta 1300*, 5.
Roig, T., Bäckman, P., & Olofsson, G. (1993) *Acta Chem. Scand. 47*, 899.
Reiss, Y., Brown, M. S., & Goldstein, J. L. (1992) *J. Biol. Chem. 267*, 6403.
Rose, I. A. (1980) *Methods Enzymol. 64*, 47.
Roskoski, R., Jr., Ritchie, P., & Gahn, L. G. (1994) *Anal. Biochem. 222*, 275.
Russo, A., & Bump, E. A. (1988) *Methods Biochem. Anal. 33*, 165.
Schafer, W. R., Kim, R., Stern, R., Thorner, J., Kim, S.-H., & Rine, J (1989) *Science 245*, 379.
Schafer, W. R., Trueblood, C. E., Yang, C.-C., Mayer, M. P., Rosenberg, S., Poulter, C. D., Kim, S.-H., & Rine, J. (1990) *Science 249*, 1133.
Segal, I. H. (1975) *Enzyme Kinetics*, Chapters V and IX, John Wiley, New York.
Sturtevant, J. M. (1955) *J. Am. Chem. Soc. 77*, 255.
Tinoco, I., Jr., Sauer, K., & Wang, J. C. (1995) *Physical Chemistry. Principles and Applications in Biological Sciences*, 3rd ed., Prentice Hall, Englewood Cliffs, NJ.
Vogt, A., Sun, J., Qian, Y., Tan-Chiu, E., Hamilton, A. D., & Sebti, S. M. (1995) *Biochemistry 34*, 12398.
Williams, B. A., & Toone, E. J. (1993) *J. Org. Chem. 58*, 3507.
Wiseman, T., Williston, S., Brandts, J. F., & Lin, L.-N. (1989) *Anal. Biochem. 179*, 13.
Zhang, F. L., Fu, H.-W., Casey, P. J., & Bishop, W. R. (1996) *Biochemistry 35*, 8166.
Zimmerle, C. T., & Frieden, C. (1989) *Biochem. J. 258*, 381.

BI9629182